Journal of Materials Chemistry A

Accepted Manuscript

ROYAL SOCIETY OF CHEMISTRY

www.rsc.org/materialsA

Journal Name

ARTICLE

Highly Adsorptive Graphene Aerogel Microsphere with Center-diverging Microchannels Structure

Received 00th January 20xx,
Accepted 00th January 20xx

DOI: 10.1039/x0xx00000x

www.rsc.org/

Shuchi Liao [a], Tianliang Zhai[a] and Hesheng Xia*[a]

The graphene oxide aerogel microspheres were prepared by a novel approach, i.e. combination of electrospraying and freeze-casting. The unique well-defined "center-diverging microchannels" dandelion-like structures were observed in the aerogel microspheres and a formation mechanism of the structure, i.e. radial–directional freezing-thawing was proposed. After further thermal reduction, the reduced graphene oxide aerogel microspheres were obtained and the center-diverging microchannels structures can be remained. Due to its highly porous, hierarchical and hydrophobic structure as well as randomly packing effect, the aerogel microspheres possess excellent adsorption ability for various organic solvents and oils, showing their potential applications in environmental pollutant treatment.

Introduction

Integrating graphene sheets into three-dimensional (3D) macroscopic structures can not only maximally remain the accessible surface areas but also construct highly porous and hierarchical architectures[1], which have practical potential applications in the fields of catalysis[2-4], energy storage and conversion[5-8], environmental pollutant treatment[9-12], biotechnologies[13-15], and composite[16, 17]. Among graphene-based macroscopic structures, graphene aerogels, which were reported early by Mann[18] and Wang[19], have become an important archetype because they combined the outstanding intrinsic properties of graphene and exciting properties (lightweight, low dielectric permittivity, etc.) of aerogel with unique topological porous structure. Over the past few years, graphene aerogels have been extensively investigated and the fabrication procedures can be summarized as follows: (1) template-directed chemical vapour deposition (CVD)[20, 21]; (2) self-assembly by using graphene oxide (GO) as precursor, mainly including cross-linking agent assisted self-assembly[22,23], hydrothermal reduction self-assembly[24,25] and chemical reduction self-assembly[2,26,27], and 3) template-directed assembly method by employing various types of templates such as polymer colloidal particles[28], organic solvent[29] and ice[18, 30]. Compared to CVD strategy which is energy-consuming and self-assembly method which generally produces disordered porous architectures, the template-directed assembly method can result in novel micro-geometry conferring the aerogel inimitable structures and properties in a facile and inexpensive way. For instance, Li et al. reported an ultralight graphene-based cellular monolith by directional freeze-casting of an aqueous dispersion of partially reduced graphene oxide[30]. Its superior elastic property is attributed to the continuous honeycomb-like network which is formed by ice crystals growth during the freeze-casting process before reduction.

Meanwhile, due to its intrinsic hydrophobic property and porous structure, graphene aerogel is an ideal candidate for environment pollution management, especially for pollutants adsorption[12,31]. For example, Li et al. prepared ultra-light, compressible and fire-resistant graphene aerogel by a one-step ethylenediamine reduction self-assembly method[32]. The aerogels exhibited not only a high absorption for diverse organics but also high speed and can be easily recycled by facile absorption–squeezing cycles. Xu et al. fabricated superhydrophobic neat graphene aerogel by chemical reduction self-assembly method and used L-phenylalanine as a reducing agent[33]. The absorption capacity of this superhydrophobic and superoleophilic graphene aerogel was higher than 100 g g^{-1} for all employed organic solvents. Ruoff et al. reported that "spongy graphene" prepared by hydrothermal reduction of GO could act as high-efficient and low-cost absorbent for oils and organic solvents[34] and recently they demonstrated a brand-new spongy graphene with an enhanced performance as an oil absorbent by high-temperature reduction and soot treatment[35]. However, until now almost all literatures about graphene aerogels applied in water treatment were macro-form monolith and focused on superhydrophobic modification and/or pore structure optimization for improving the performance of adsorption, and the effects of shape and size of graphene aerogel on the performance were neglected.

On the other hand, shaping aerogel into microspheres, that is, aerogel microspheres or microaerogel, may open up

[a] State Key Laboratory of Polymer Materials Engineering, Polymer Research Institute, Sichuan University, Chengdu, 610065, China .E-mail: xiahs@scu.edu.cn.

† Footnotes relating to the title and/or authors should appear here.
Electronic Supplementary Information (ESI) available: [details of any supplementary information available should be included here]. See DOI: 10.1039/x0xx00000x

potential applications such as superabsorbent, drug/catalyst carriers, functional composite particles, filtering membrane, etc. [36-38] For example, Areerat et al. successfully synthesized carbon aerogel microspheres by employing sol–gel polycondensation of a resorcinol–formaldehyde solution, which exhibited excellent adsorption capacity of phenol[39]. Deng et al. adopted a facile spray-freeze-drying method to fabricate aerogel microspheres from natural cellulose nanofibrils and it was used as novel cell culture scaffold which showed low bulk density, high moisture rate, and high water absorption capacity[40].

Inspired by the pioneering developments of aerogel microspheres, we consider that graphene microaerogel may provide another possibility in enhancing the performance of graphene aerogel in the field of pollutants adsorption.

Herein we reported for the first time graphene oxide aerogel microspheres (GOAMs) with a novel "center-diverging microchannels" structure obtained by a novel approach, i.e. combination of electrospraying and freeze-casting. The relatively uniform GOAMs can be obtained, and the size of aerogel microspheres can be easily tuned by adjusting the parameters of electrospray processing. Furthermore, the reduced graphene oxide aerogel microspheres (rGOAMs) were prepared by a two-step thermal reduction process without breaking the "center-diverging microchannels" structures. The resulting rGOAMs exhibited quite high adsorption capacities and fast adsorption rate as well as excellent recyclability, when used as sorbent for various organic solvents and oils. We expect that the graphene aerogel microspheres can provide more possibilities for fabrication and applications of graphene-based materials and our proposed approach also can be extended to prepare other aerogel microspheres except graphene.

Experimental

Materials

Flake Graphite (~75 μm) was obtained from Qingdao Tianhe Graphite Co. Ltd (China). Concentrated sulfuric acid (H_2SO_4) and hydrochloric acid (HCl) were all of analytical-grade and obtained from Sichuan Xilong Chemical Co. Ltd (China). Potassium permanganate ($KMnO_4$), acetic ether and n-hexane were obtained from Chengdu Kelong Chemical Reagent Company (China).

Preparation of graphene oxide aqueous dispersion

The preparation of graphite oxide was according to our previous work[41]. Graphene oxide (GO) aqueous dispersion was obtained by sonication for 1h in an ultrasonic cleaner（50 W, 40 kHz） and then mildly stirred overnight.

Preparation of GOAMs

Typically, graphene oxide aqueous dispersion (6.0 mg/ml, 10 ml) was loaded into the syringe of electrospraying device (Beijing Yongkang Co. China). A flask with n-hexane put into a Dewar bottle which is filled with liquid N_2/ethyl acetate slush bath (-85 ^{o}C) was used as the collector for the microdroples resulted from the electrospraying of GO dispersion. The electrospraying parameters are as follows: the flow rate of GO dispersion: 7.5 mL/h; the electrospraying voltage: 8 kV; the distance between the tip of the syringe to the surface of the collector liquid: 10 cm. Then liquid droplets of GO aqueous dispersion from electrospraying sprue will immediately convert to GO ice microspheres once sprayed into the cold hexane collector. The cold GO microspheres/hexane was quickly filtered and then lyophilized at -50 ^{o}C with a reduced pressure of less than 20 Pa for 24 h to obtain the graphene oxide aerogel micropspheres (GOAMs).

Preparation of the reduced GOAMs (rGOAMs)

A two-step thermal reduction process was conducted. GOAMs was sequentially heated in a vacuum oven for 60 min at 120 ^{o}C, 60 min at 150 ^{o}C, and 120 min at 180 ^{o}C, then put the pre-reduced microspheres into a microwave oven and further heated for 1 min at a power of 700 W in the atmosphere of Ar to get the rGOAMs.

rGOAMs uptake for organic solvents and oil

Firstly, a small amount of organic solvents or oils were placed in a container. An excessive rGOAMs used for the adsorption test was weighed and recorded as m_0. Then the rGOAMs was gradually added into the liquid to adsorb, until all liquid was taken up (no flowing was observed). The left unused rGOAMs and the used rGOAMs with adsorbed liquids were weighed and recorded as m_1 and m_2, respectively. The mass of used rGOAMs for adsorption is m_0-m_1. Therefore, the adsorption Q value (g/g) is calculated by the following formula (1):

$$Q = [m_2-(m_0-m_1)] / (m_0-m_1). \quad (1)$$

The rGOAMs recycling

To obtain the recycled rGOAMs samples after absorbing the solvent or oil by using two methods: (1) Evaporation: the n-hexane-adsorbing aerogel microspheres were dried at 70 ^{o}C in an oven for at least 1h. (2) Combustion: the diesel-adsorbing aerogel microspheres were burned up. These samples were carried out the same uptake test again as mentioned above.

Characterizations

The packing densities of the GOAMs and rGOAMs were calculated by their mass-to-volume ratios. The volume was determined by filling a certain volume cylinder with GOAMs or rGOAMs and the mass was recorded by an electronic balance (METTLER TOLEDO, AL104). The Digital pictures were taken by Digital Microscope (VHX-1000, Keyence, Japan) and SEM images were recorded by a Scanning Electron Microscope (JSM-5900LV, JEOL, Japan). Grading analysis was carried out by a Particle Size Analyzer (Mastersizer 2000, Malvern, Britain) equipment using GOAMs sample which has heated in vacuum oven at 180 ^{o}C for 2h and is stable in the testing solvent.

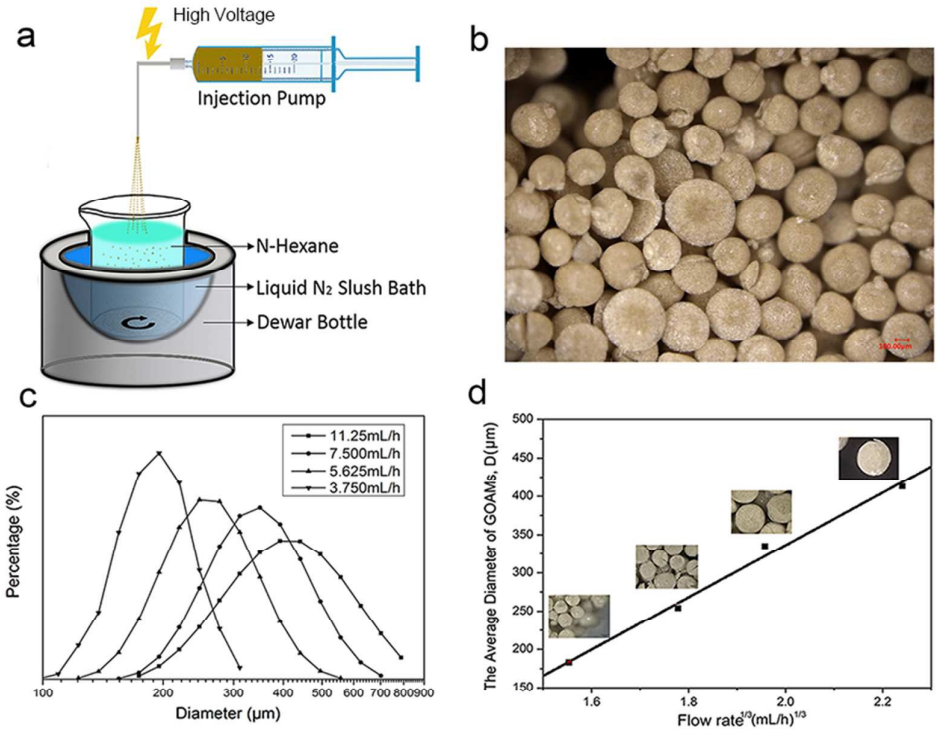

Fig 1. (a) Schematic diagram for our approach, i.e. electrospraying combined with freeze-casting process; (b) Typical digital microscope images of the prepared GOAMs (experiment conditions: applied voltage: 8 kV; distance between electrodes: 10 cm; GO concentration: 6.0mg/ml);(c) Grading analysis of GOAMs prepared at different flow rates of GO dispersion (GO dispersion concentration: 6.0mg/ml; distance between electrodes: 10 cm; applied voltage: 8 kV); (d Linear fitting of diameter of GOAMs with flow rate1/3 of GO dispersion (insets are the typical optical pictures of GOAMs made at different flow rates).

Fourier-Transform Infrared (FT-IR) spectroscopy was recorded on a Nicolet 560 FT-IR spectrometer, FT-IR measurements were conducted in a transmission mode in KBr pellets. Raman spectra were conducted on VERTEX 70 (Bruker, Germany). XPS measurements were carried out using an instrument (XSAM800, Kratos, Britain). Charge effects were compensated assuming carbon C1s peak at 284.8 eV position. For XRD, The samples including GO, GOAMs and rGOAMs were mounted individually into a Philip-X'Pert X-ray diffractometer fitted with a goniometer detection device (anode 40 kV, filament current 35 mA). Contact angle (CA) measurements were performed by a contact angle meter (Kruss, DSA25). Typically, 4 μL water droplet was placed on the surface of a film made by pressing GOAMs or rGOAMs, and repeated for three times. The average value was taken as the contact angle (CA). N_2 adsorption/desorption experiments were recorded by an Automatic Surface Area and Porosity Analyzer (Tristar II 3020, Micromeritics, USA) through a test tube filled with rGOAMs.

Results and discussion

Preparation of GOAMs by electrospraying and freeze-casting

Figure 1a is the schematic diagram for our approach, i.e. electrospray combined with freeze-casting, to fabricate the GO aerogel microspheres. The GO dispersion was loaded into a syringe of the electrospray device (Figure S1) and the needle of the syringe was connected with a high voltage to form an electric field, which charged the GO dispersion droplet located on the tip of needle. With a sufficient high voltage, the charged droplet was stretched to form a well-known "*Taloy cone*" [42], the thin jet erupted from "*Taloy cone*" eventually broke up into a steam of smaller charged droplets, which were collected into a container filled with cold n-hexane (-85 ^{o}C -45 ^{o}C) that could keep low temperature for at least 2.5 h by liquid N_2 slush bath to form the GO/ice microspheres. Then the solvent was removed by rapid filtration. The filtered solid powder samples were lyophilized to remove the frozen water slowly from the GO/ice microspheres and finally the GOAMs were formed as shown in Figure 1b.

The electrospraying technology is a size-controllable method for preparation of microspheres. In order to obtain microspheres with standard spherical shape and uniform size, we systematically investigated and optimized the parameters of electrospraying process. We found that the flow rate was a key factor for the size control. Figure 1c shows that the size and size distribution of GOAMs apparently increase as the flow rate increases. The average diameter of GOAMs increases from ~183 to ~413 μm when the flow rate increases from 3.75 to 11.25 mL/h. Loscertales[43-45] reported a scaling law for droplets size erupting from "*Taloy cone*" during electrospraying as follows:

$$d = \alpha \left(\frac{q\varepsilon_0\varepsilon_r}{K}\right)^{\frac{1}{3}} \quad (2)$$

Where d is the diameter of droplet, ε_0 represents the vacuum permittivity, ε_r represents the relative permittivity of the liquid, K is the conductivity of liquid, q is the flow rate, α is a constant. This formula reveals that the flow rate and liquid properties determine the size of the microspheres. In our case, as shown in Figure 1d, the average diameter for GOAMs resulted from the *Taloy cone* droplets is indeed proportional to $q^{1/3}$, fitting very well with the scaling law. This result suggests that electrospray can realize size-controllable fabrication of GOAMs by adjusting the flow rate of the GO dispersion during spraying process. For other parameters, the electrospray voltage, and the distance between the tip of the needle to the surface of the target liquid in the container are very important and must be adjusted to obtain the desired GOAMs (more details shown in Figure S2). The concentration of GO dispersions has no significant effect on the size of GOAMs (Figure S3). This can be understood by the above scaling law, because GO dispersions have stable liquid properties, such as the permittivity of the liquid (ε_r) and the conductivity of liquid (K) no matter the GO concentration.

Structure and formation mechanism of GOAMs

We observed the surface morphology of GOAMs obtained from different GO dispersions by SEM. Figure 2a-d shows that the GOAMs made by our approach present perfect spherical shape (Figure 2a and c) and also the highly porous network featured by randomly interconnected crumpled GO sheets can be found (Figure 2b and d, inset image of Figure 2d: graphene oxide sheet on the surface of GOAMs). The GOAMs obtained at a GO concentration of 4.0 mg/ml has a larger pore size of ~15 μm and looser pore structures (Figure 2a and b) in the surface of GOAMs, compared to the sample obtained at a GO concentration of 6.0 mg/ml (Figure 2c and d). For electrospraying, the change of the GO concentration in the dispersion has little influence on microsphere's size as shown above, but has significant effects on the pore microstructures. The GO dispersion of lower GO concentration contains less amounts of GO sheets, therefore leading to looser pore structures and larger pore size in GOAMs. In addition, Figure 2b and d show that the "crosslinking points" (marked with red circles) of the GOAMs were formed due to the partial overlapping of GO sheets caused by squeezing effect of ice crystals. The crosslink points are very important to make the GOAMs stable after drying, which means a critical concentration of GO dispersion is necessary for GOAMs preparation. The decrease in GO concentration could lead to lower mechanical strength of the GOAMs mainly due to the decrease of "crosslinking points". In our case, if the GO concentration is lower than 3.5 mg/ml, it is not successful to obtain the stable GOAMs.

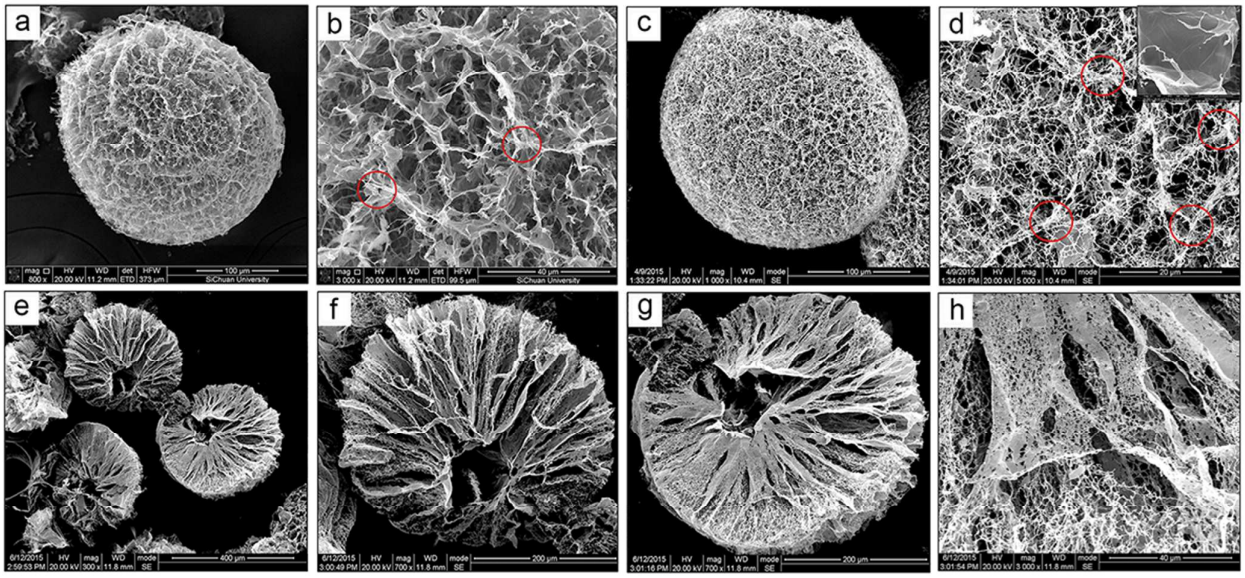

Fig 2. (a-b) SEM images of typical GOAMs made from a GO concentration of 4.0 mg/ml (a: lower magnification; b: higher magnification); (c-d) SEM images of typical GOAMs made from a GO concentration of 6.0 mg/ml (c: lower magnification; d: higher magnification); (e-h) SEM images of GO aerogel hemispheres made by cracking GO ice microspheres obtained with a GO concentration of 6.0 mg/ml (e: lower magnification; f, g: medium magnification; h: higher magnification)

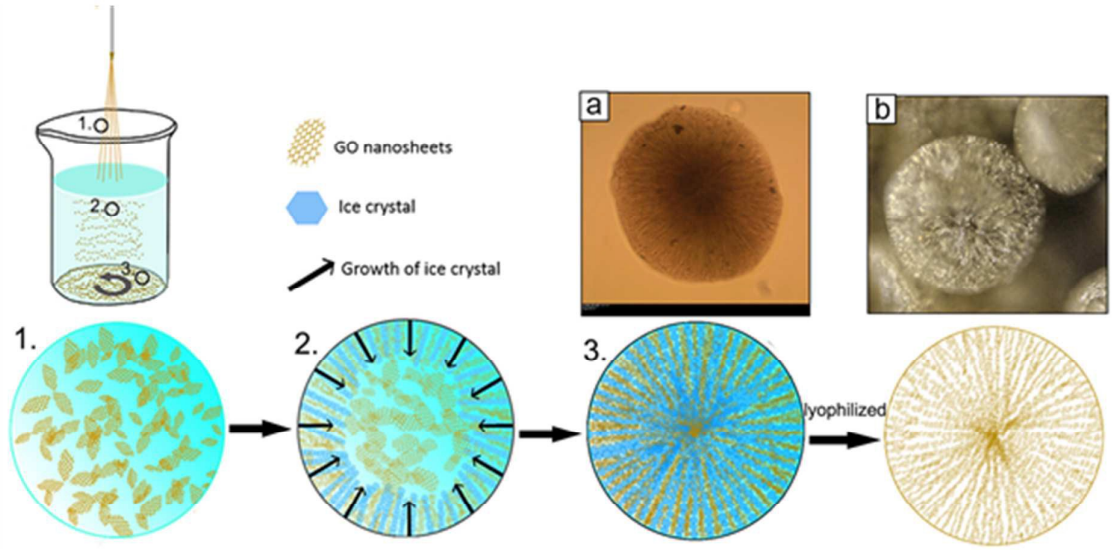

Scheme 1. Schematic illustration for the formation mechanism of GOAMs, i.e. radial-directional freezing-thawing. (a) Optical images of GOAMs; (b) Typical digital images of GOAMs.

The packing density of GOAMs is measured. For GOAMs made from 6.0 mg/ml and 4.0 mg/ml GO dispersion, the packing densities were 3.90 mg/cm^{-3} and 2.88 mg/cm^{-3}, respectively. Both of them fall into the category of ultralight materials[46]. Since the mechanical strength and stability of the GOAMs decrease with a decrease in GO concentration, we finally chose 3.90 mg/cm^{-3} GOAMs for use in the following studies.

Furthermore, we observed the inner microstructure of GOAMs by cracking the GO ice microspheres before lyophilization. The SEM pictures of resulting hemispheres are shown in Figure 2e-h. Surprisingly, we found a unique ordered center-diverging microchannels structure in GOAMs, which looked like dandelion. The microchannels emit from the center of microspheres can be clearly observed in Figure 2e, f and g, which are wrapped by thin-walls of multilayer-stacked graphene oxide sheets with a dimension of several microns. The dandelion-like hemispheres is so pretty and exquisite beyond our expectation. Also it can be noted that inside the channels there are hierarchical pores with size distributions from sub-microns to microns (Figure 2h). The center-diverging microchannels structure also can be observed by optical microscopy (Scheme 1a and b, and Figure S4). Few literatures demonstrated such a novel inner structure of microsphere but it is worth noting that Yang et al. prepared chitosan spheres with radial-like macro pores[47]. They presumed that the formation of such macro pores was due to the interaction of iron-oxide co-precipitation with chitosan gelation and without the participation of iron-oxide or gold nanoparticles, the macroporous structures were not existed. Clearly, their principle is different from ours, in which no any added substances in GO dispersions are needed to obtain the center-diverging microchannels structure.

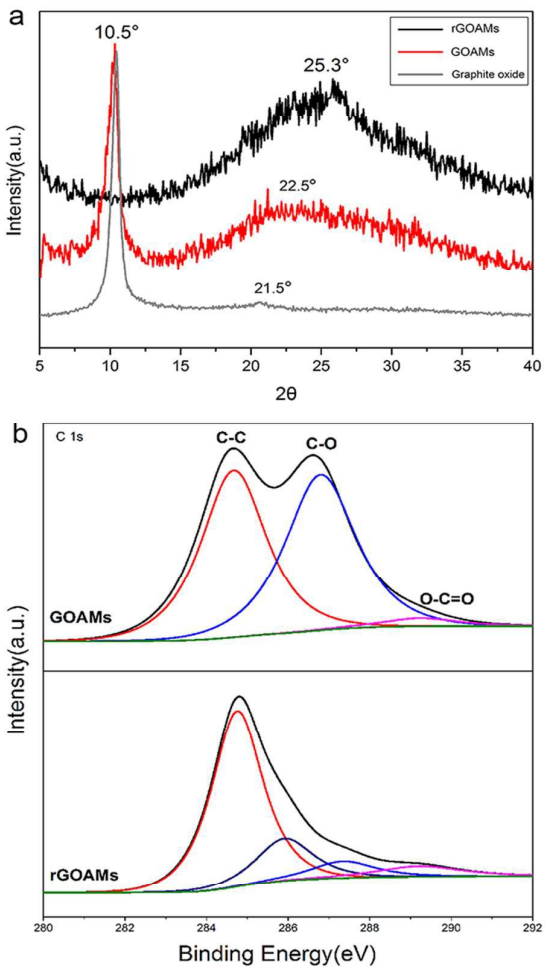

Fig 3. (a) XRD pattern of graphite oxide, GOAMs, rGOAMs (b) C 1s spectrum of XPS for GOAMs and rGOAMs, respectively

Scheme 1 demonstrated the proposed formation mechanism of such a unique microchannels structure in GOAMs. Firstly, because of the strong hydrophobicity and low surface tension of the liquid collector such as n-hexane, the splitting droplets consisting of GO sheets and water can remain its spherical shape when falling into the cold liquid collector (Step 1). Then immediately the droplets surface contacted with the liquid of extremely low temperature of liquid N_2 slush bath, the water in the droplets surface begins to crystallize firstly to form the ice (Step 2). Under stirring, the spherical microdroplets evenly cool from the surface to the interior so that ice crystals grow along the radial directions into the droplet center and squeeze the GO sheets to stack and orient (Step 3 and Scheme 1a), and finally form porous microchannels structure after the ice crystals were removed through a slow lyophilizing process (Scheme 1b). The mechanism can be defined as "Radial–directional Freezing-Thawing", which is different from the directional-freezing mechanism developed by Rannard and Cooper[48]. The principle can be used to prepare dandelion-like microspheres of various raw materials with well-defined "center-diverging microchannels" structure. These microspheres with interesting inner structure may possess exciting potential applications such as cell culture or chromatographic column packing or versatile catalyst by loading on functional nanoparticles.

Thermal reduction to obtain rGOAMs

In order to restore the excellent properties of graphene, the GOAMs were further reduced to form the reduced graphene oxide aerogel microspheres (rGOAMs). A two-step thermal reduction method, i.e. heating pre-reduction and microwave post-reduction was used to ensure the reduced rGOAMs remaining its unique architecture as well as achieving a relatively high reduction degree[49-51].

XPS XRD, FTIR and Raman spectroscopy were used to characterize the chemical transition of GOAMs to rGOAMs. XRD analysis is shown in Figure 3a. The characteristic sharp diffraction peaks at 2θ~10.5°were observed for graphite oxide and GOAMs samples. The calculated interlayer distance is ~0.84 nm, which should be attributed to the existence of hydroxyl, epoxy, and carboxyl groups between the graphite oxide sheets. Meanwhile, graphite oxide has a weak peak at 2θ~21.5°, which is close to the peak of pristine graphite (0.34 nm).This is attributed to an incomplete oxidation of graphite. The GOAMs also have a broad peak around 2θ~22.5°, this may be attributed to the partial stacking of graphene oxide sheets which were incomplete oxidized due to the squeezing effect of the ice crystals. While for the reduced sample rGOAMs, the peak at 2θ~10.5° disappears, and a broad peak at 2θ~25.3° appears, corresponding to a layer spacing of ~0.35 nm, which attributes to re-stacking of graphene layer in rGOAMs and

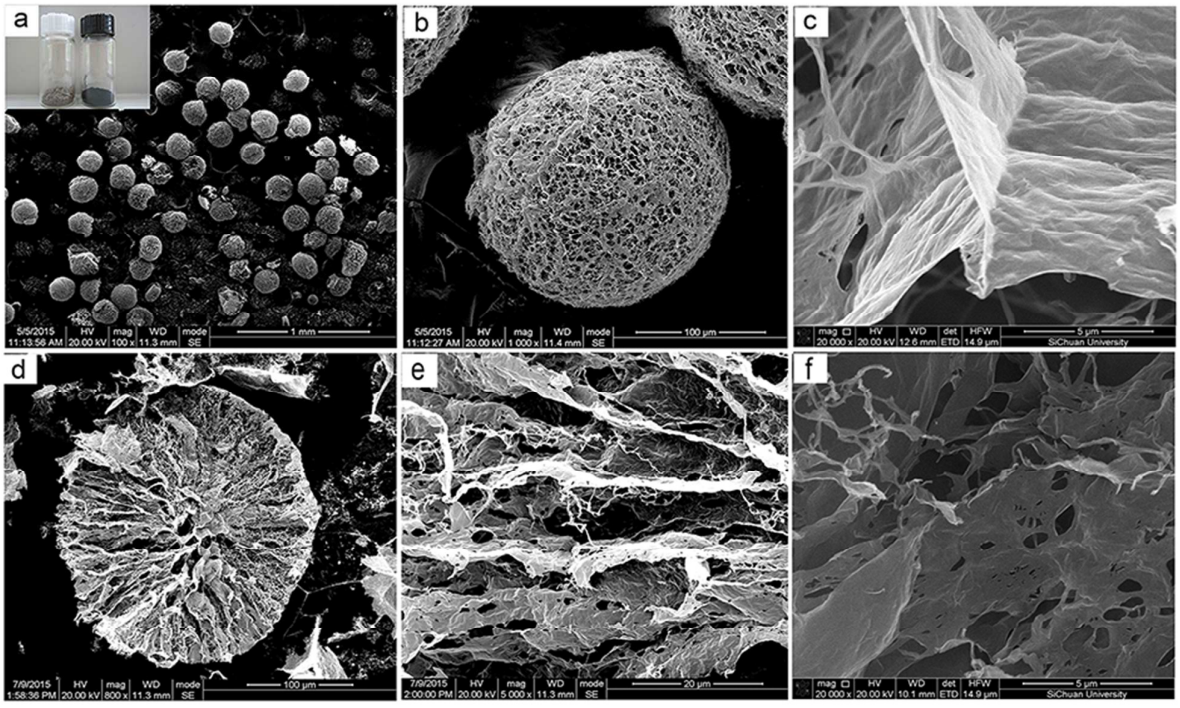

Fig 4. Typical SEM images of (a-b) rGOAMs and (c) restacking of graphene sheets on the surface of rGOAMs; SEM images of (d) the rGO aerogel hemispheres ; (e) the center-diverging microchannels of rGOAMs ; (f) the wall of microchannels

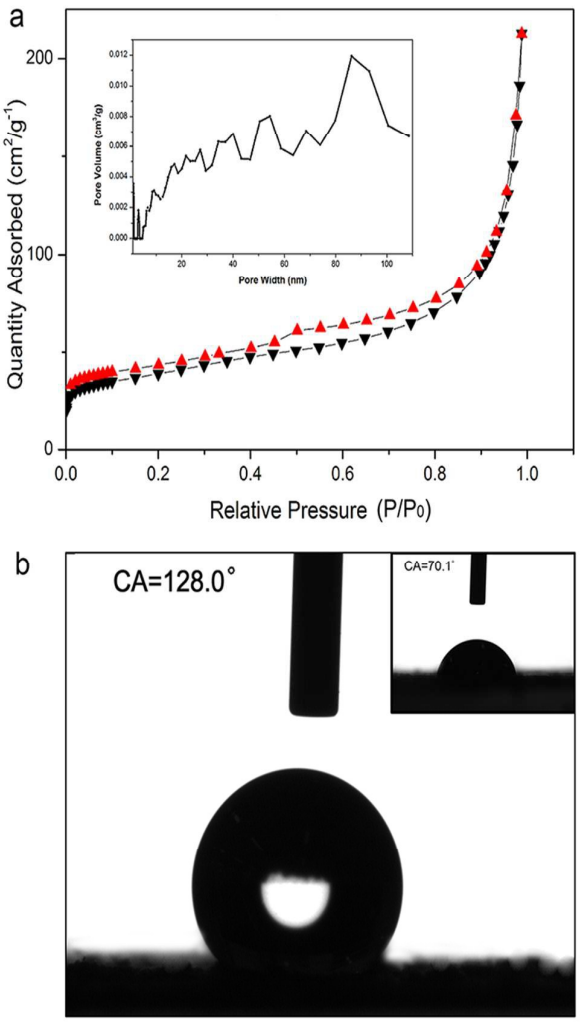

Fig 5. (a)N_2 adsorption/desorption isotherms (inset: the pore size distributions for rGOAMs); (b) optical images of a water droplet on the surface of rGOAMs and GOAMs (inset image).

indicated the efficient de-oxygenation of GO sheets.[52] Figure 3b shows the C1s spectra of XPS for GOAMs and rGOAMs. The peak at 286.8 eV is typically assigned to C-O species of graphene oxide[53]. After thermally reduction, the peak of C-O species at ~286.8 eV nearly disappears and the elemental ratio of C/O for GOAMs and rGOAMs analysed by XPS is ~2.1 and ~8.1 respectively, which confirms the efficient reduction. FTIR results (Figure S5) show that GOAMs have four main peaks at 1625, 1050, 1227 and 1726 cm^{-1}, corresponding to the skeleton vibration of aromatic C=C, deformation stretches of C-O (alkoxy/alkoxide), stretching vibration of C-O (epoxy/ether) and C=O (carbonyl), respectively [54]. For rGOAMs, the peaks at 1050, 1227, 1726 cm^{-1} weakened remarkably, suggesting that the oxygen-containing groups were significantly removed after reduction. Raman spectra (Figure S6) show that both GOAMs and rGOAMs have the characteristic D and G bands, and the calculated different intensity radio of I_d/I_g for rGOAMs increases from 0.92 to 1.01, indicating that fewer defects and more sp^2 domains were formed in rGOAMs after reduction [55].

Structure and properties of rGOAMs

Figure 4a-f are the SEM images of rGOAMs and rGO aerogel hemispheres (the inset pictures of Figure 4a are from the brown GOAMs and the black rGOAMs sample after reduction). The two-step reduction procedure has little influence on the shape or inner structure of these aerogel microspheres. The rGOAMs remain spherical shape with highly porous network (Figure 4a-b) as well as the unique hierarchical center-diverging microchannels architectures (Figure 4d-e). From Figure 4c we clearly observed the re-stacking of graphene sheets after reduction, which is consistent with the results of XRD. Figure 4e-f showed that after thermal reduction, the wall of microchannels have more ruffles and pores comparing to Figure 2h, which may increase the roughness of the microchannels.

Then, N_2 adsorption/desorption experiments are tried to evaluate the porosity properties of rGOAMs. As shown in Figure 5a, the analysis results based on Brunauer-Emmett-Teller (BET) and Barrett–Joyner–Halenda (BJH) model reveal that the rGOAMs exhibit a type IV isotherm with a pore width of 4-100 nm. It should be pointed out that it is difficult to conduct the BET test for aerogel microspheres because they were so light that we must compress them in order to gain enough mass in the test tube for the measurement. As a result, the BET test showed a relatively low specific surface ca.140.4375 cm^2/g and a pore volume of 0.33 g/cm^3 compared to other ice-templating graphene 3D architectures[56, 57]. However, even after compression, these data can still reflect the porous structure of the rGOAMs remaining after reduction.

The water contact angle was measured to evaluate the hydrophobicity of rGOAMs. As shown in Figure 5b, the contact angle of GOAMs is 70.1° and after reduction, the contact angle of rGOAMs turned to 128.0°. The relatively high hydrophobicity of rGOAMs can be attributed to the restoration of π-π conjugate structure and the roughness of the graphene sheets (Figure 4e-f) after thermal reduction, especially microwave treatment[50, 51].

Also, the packing density of rGOAMs made from 6mg/ml GO dispersion is measured and the result is 2.8 mg/cm^{-3}, showing its feature of lightweight.

Solvent/oil uptake performance of rGOAMs

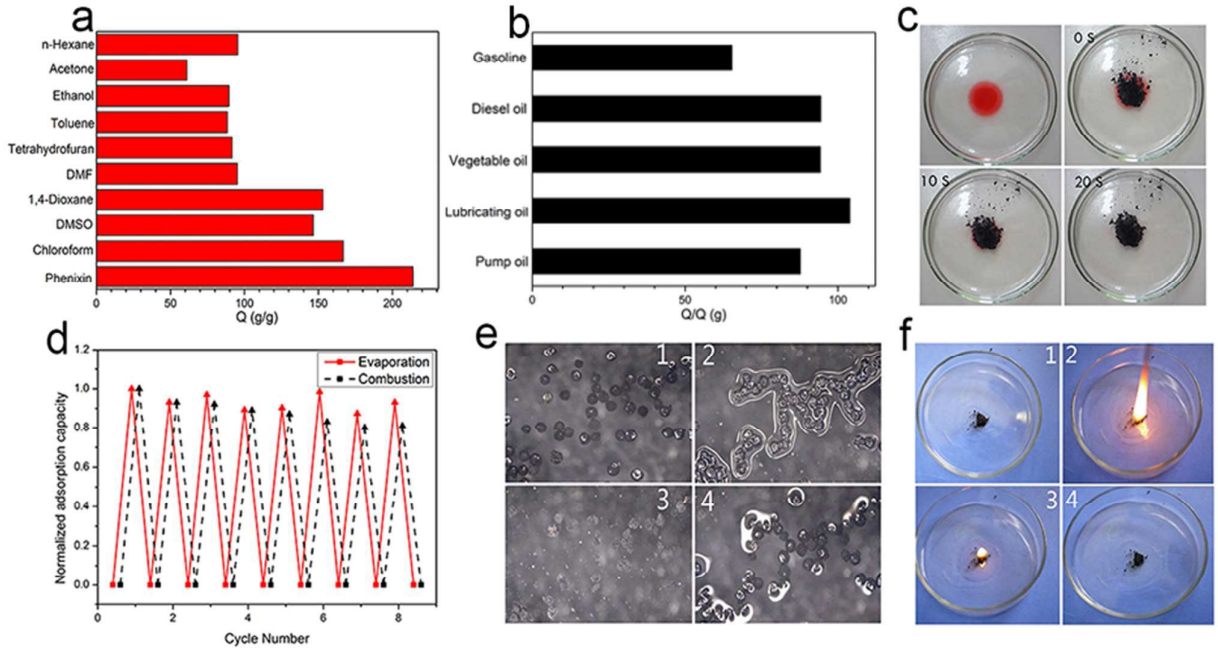

Fig 6. (a-b) Absorption capacities of rGOAMs for a range of organic liquids and oils; (c) Absorption process of pump oil (dyed with Sudan red III) in water by the rGOAMs within 20s; (d) Recyclability of rGOAMs for the absorption of n-hexane and diesel oil under evaporation and combustion cycles, respectively; (e) Pictures of evaporation process of n-hexane adsorbed rGOAMs (recorded by digital microscope); (f) Pictures of combustion process of diesel oil adsorbed rGOAMs.

The rGOAMs are supposed to be an ideal candidate as sorbent due to their strong hydrophobic, large specific surface, and the highly hierarchal structure with novel center-diverging microchannels. It can be understood that the center-diverging microchannels can play an important role for garnering the absorbed liquids as well as improving the uptake rate due to the capillary effect. Figure 6a shows that the adsorption capacities of rGOAMs for 10 kinds of organic solvents are very high, in the range of 60~214 g g^{-1}. The adsorption for Phenixin is highest, ~214 g g^{-1} and for Acetone is lowest, ~60 g g^{-1}. Figure 6b shows that the adsorption capacities of rGOAMs for 5 kinds of oils are in the range of 62~105 g g^{-1}. The adsorption capacity for different organic liquids depends on densities of the liquids. An increase in organics densities means a larger amount of organics can be stored in the void space. As shown in Figure S7, the adsorption capacities of rGOAMs for different organic liquids are roughly proportional to the density of the solvents, which is the similar to previous reports[32, 33, 57]. The adsorption capacities of rGOAMs are much higher than those of conventional adsorptive materials such as expanded graphite, activated carbon, polymeric absorbents[57], and also higher than graphene sponge[11], rGO foam[58,59], graphene/CNTs aerogel[60, 61], as well as other graphene hybrid aerogels[2, 62, 63], and comparable to superhydrophobic graphene aerogels[32, 33], as summarized in Table S1. In addition, Figure 6c and Movie S1 show that 0.6 g pump oil (dyed with Sudan Red III) floating on the water can be quickly absorbed by a spoonful of rGOAMs (ca. 6 mg) within 20 s, which indicating an adsorption rate of 5 g g^{-1} s^{-1}, much faster than the previous reported *in-situ* reduced all-graphene sponge (0.57 g g^{-1} s^{-1}) [34].

After adsorption, the rGOAMs can be easily collected and recycled by two kinds of methods, i.e. evaporation and combustion. Digital pictures Figure 6e and Movie S2 showed the evaporation procedure of ethanol-adsorbed rGOAMs. We can observe that the rGOAMs filled with ethanol have a well-defined spherical shape in Figure 6e picture 1 while these microspheres slowly shrink during the evaporation process (Figure 6e picture 2) and finally become irregular particles (Figure 6e picture 3), but to our surprise, these particles swell up and restored the original spherical shape after the re-adsorption which behaves like “organogels” (Figure 6e picture 4). This phenomenon indicates the rGOAMs have a stable and flexible network structure. The rGOAMs can also be recycled by combustion. As shown in Figure 6f and Movie S3, the diesel oil can be quickly removed from rGOAMs sample by combustion (Figure 6f pictures 1-3) while the sample can remain its original sample shape nearly without mass loss (Figure 6f picture 4) after combustion which indicated the rGOAMs have high enough specific surface areas for fast heat dissipation. Figure 6d showed that the rGOAMs can remain ~90% and ~80% adsorption capacity even after 8 times cycles by evaporation or combustion respectively. Moreover, the rGOAMs is lightweight enough to be spreadable over large areas, which is especially helpful for the treatment of oil spilled at sea. All these features make the rGOAMs possess

promising application in environmental pollutant management.

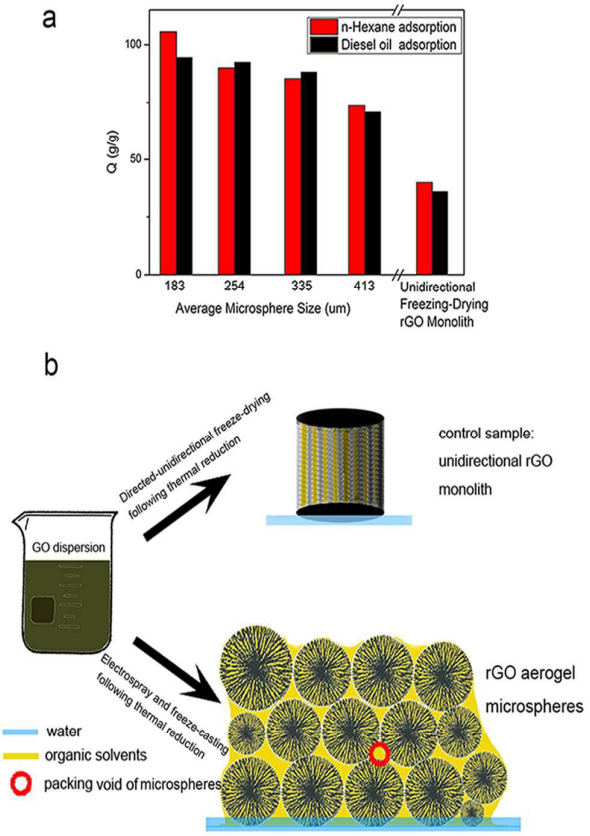

Fig 7. (a) Absorption capacities of rGOAMs with different average sizes and rGO monolith foam (b) Proposed mechanism for advanced uptake performance of rGOAMs: randomly packing effect

The adsorption mechanism for rGOAMs

We investigated the size effect of rGOAMs on the adsorption capacity. As shown in Figure 7a, with decreasing the diameter of rGOAMs, the Qs value increases due to the increase in the specific surface area and the active sites for the attachment of organic small molecules. More importantly, we compared the adsorption property for rGOAMs and the graphene monolith foam fabricated by unidirectional freezing-dry technology following the same two-step thermal reduction (Figure S8). From Figure 7a it can be noted that the unidirectional freezing-drying rGO monolith foam has a lower adsorption capacity for n-hexane and diesel oil compared to the rGOAMs.

The enhanced adsorption performance of rGOAMs can be attributed to the randomly packing effect of microspheres as illustrated in Figure 7b. During the packing of graphene aerogel microspheres, the new void space among the microspheres can be produced, which can store more organic liquids. The ratio for intrinsic volume to randomly packing volume of spheres is around 0.6-0.64 according to the references[64, 65], which means that the void space among spheres is about 40% of whole packing volume of spheres. This can also be understood by the difference of densities between rGO monolith foam and randomly packed rGOAMs. The density of rGO monolith foam was measured as 4.38 mg/cm^3. In our case the rGO monolith foam and the rGOAMs are made from the same GO dispersion with a concentration of 6 mg/ml thus the density for rGO monolith foam and the individual graphene microsphere should be the same. The calculated density for the packed graphene aerogel microspheres is 3.112 mg/cm^3, if taking the void space volume as 40% of whole packing volume of spheres, which is close to our determined packing density, ~2.8 mg/cm^3, much lower than that for rGO monolith foam. Accordingly, it can be understood that rGOAMs have better adsorption performance than rGO monolith foam in terms of such randomly packing effect originated from microspheres.

Conclusions

In conclusion, the novel graphene oxide aerogel microspheres with a unique well-defined "center-diverging microchannels" microstructure were prepared through a novel approach, i.e. electrospray combined with "radial-directional" freeze-casting. The morphology and size of aerogel microspheres can be easily controlled by adjusting the parameters of electrospraying. A formation mechanism of the aerogel microspheres, i.e. radial–directional freezing-thawing was proposed. After a two-step thermal reduction, the lightweight rGO aerogel microspheres were obtained with the "center-diverging microchannels" microstructure remained. Due to its highly porous, hierarchical and hydrophobic structure as well as randomly packing effect, The rGOAMs exhibit excellent adsorption capability for various organic solvents and oils, as high as 60~214g.g^{-1}, showing potential applications in environmental pollutant treatment, water purification, etc.

Acknowledgements

This work is supported by International Science & Technology Cooperation Program of China (2015DFA51110).

Notes and references

1. L. Liu, Z. Niu, L. Zhang and X. Chen, *Small*, 2014, **10**, 2200-2214.
2. T. Wu, M. Chen, L. Zhang, X. Xu, Y. Liu, J. Yan, W. Wang and J. Gao, *J. Mater. Chem. A*, 2013, **1**, 7612.
3. H. Yin, C. Zhang, F. Liu and Y. Hou, *Adv. Funct. Mater*, 2014, **24**, 2930-2937.
4. W. Yan, F. He, S. Gai, P. Gao, Y. Chen and P. Yang, *J. Mater. Chem. A*, 2014, **2**, 3605.
5. S.-H. Park, H.-K. Kim, S.-B. Yoon, C.-W. Lee, D. Ahn, S.-I. Lee, K. C. Roh and K.-B. Kim, *Chem. Mater.*, 2015, **27**, 457-465.
6. C. Hou, H. Wang, Q. Zhang, Y. Li and M. Zhu, *Adv. Mater.*, 2014, **26**, 5018-5024.

7. X. Yang, C. Cheng, Y. Wang, L. Qiu and D. Li, *Science*, 2013, **341**, 534-537.
8. S. Han, D. Wu, S. Li, F. Zhang and X. Feng, *Adv. Mater.*, 2014, **26**, 849-864.
9. G. M. Joshi and K. Deshmukh, *J. Electron. Mater*, 2014, **43**, 1161-1165.
10. Y. Han, Z. Xu and C. Gao, *Adv. Funct. Mater*, 2013, **23**, 3693-3700.
11. J. Zhao, W. Ren and H.-M. Cheng, *J. Mater. Chem.*, 2012, **22**, 20197.
12. Y. Shen, Q. Fang and B. Chen, *Environ. Sci & Technol*, 2015, **49**, 67-84.
13. A. Sahu, W. I. Choi and G. Tae, *Chem. Commun*, 2012, **48**, 5820-5822.
14. Y. Q. Li, T. Yu, T. Y. Yang, L. X. Zheng and K. Liao, *Adv. Mater.*, 2012, **24**, 3426-3431.
15. H. Liang, X. B. Zhang, Y. Lv, L. Gong, R. Wang, X. Zhu, R. Yang and W. Tan, *Accounts. Chem. Res*, 2014, **47**, 1891-1901.
16. W. Chen, S. Li, C. Chen and L. Yan, *Adv. Mater.*, 2011, **23**, 5679-5683.
17. S. Ye, J. Feng and P. Wu, *J. Mater. Chem. A*, 2013, **1**, 3495.
18. J. L. Vickery, A. J. Patil and S. Mann, *Adv.Mater*, 2009, **21**, 2180-2184.
19. J. Wang and M. W. Ellsworth, *Ecs Transactions*, 2009, **19**, 241-247.
20. Z. Chen, W. Ren, L. Gao, B. Liu, S. Pei and H. M. Cheng, *Nat Mater*, 2011, **10**, 424-428.
21. J.-C. Yoon, J.-S. Lee, S.-I. Kim, K.-H. Kim and J.-H. Jang, *Sci. Rep*, 2013, **3**.
22. H. Bai, C. Li, X. Wang and G. Shi, *Chem. Commun*, 2010, **46**, 2376-2378.
23. Q. Fang and B. Chen, *J. Mater. Chem. A*, 2014, **2**, 8941.
24. Y. Xu, K. Sheng, C. Li and G. Shi, *ACS nano*, 2010, **4**, 4324-4330.
25. L. Ren, K. S. Hui and K. N. Hui, *J. Mater. Chem. A*, 2013, **1**, 5689.
26. W. Chen and L. Yan, *Nanoscale*, 2011, **3**, 3132-3137.
27. G. Tang, Z.-G. Jiang, X. Li, H.-B. Zhang, A. Dasari and Z.-Z. Yu, *Carbon*, 2014, **77**, 592-599.
28. B. G. Choi, M. Yang, W. H. Hong, J. W. Choi and Y. S. Huh, *ACS Nano*, 2012, **6**, 4020-4028.
29. Y. Li, J. Chen, L. Huang, C. Li, J. D. Hong and G. Shi, *Adv. Mater.*, 2014, **26**, 4789-4793.
30. L. Qiu, J. Z. Liu, S. L. Chang, Y. Wu and D. Li, *Nat. Commun*, 2012, **3**, 1241.
31. S. Nardecchia, D. Carriazo, M. L. Ferrer, M. C. Gutierrez and F. del Monte, *Chem. Soc. Rev*, 2013, **42**, 794-830.
32. J. Li, J. Li, H. Meng, S. Xie, B. Zhang, L. Li, H. Ma, J. Zhang and M. Yu, *J. Mater. Chem. A*, 2014, **2**, 2934.
33. L. Xu, G. Xiao, C. Chen, R. Li, Y. Mai, G. Sun and D. Yan, *J. Mater. Chem. A*, 2015, **3**, 7498-7504.
34. H. Bi, X. Xie, K. Yin, Y. Zhou, S. Wan, L. He, F. Xu, F. Banhart, L. Sun and R. S. Ruoff, *Adv. Funct. Mater*, 2012, **22**, 4421-4425.
35. H. Bi, X. Xie, K. Yin, Y. Zhou, S. Wan, R. S. Ruoff and L. Sun, *J. Mater. Chem. A*, 2014, **2**, 1652-1656.
36. C. A. García-González, J. J. Uy, M. Alnaief and I. Smirnova, *Carbohyd.Polym*, 2012, **88**, 1378-1386.
37. Z. Ulker and C. Erkey, *J. Control. Release,* 2014, **177**, 51-63.
38. S. Yun, H. Luo and Y. Gao, *RSC Adv.*, 2014, **4**, 4535-4542.
39. J. Chaichanawong, K. Kongcharoen and S. Areerat, *Adv. Powder. Technol*, 2013, **24**, 891-896.
40. H. Cai, S. Sharma, W. Liu, W. Mu, W. Liu, X. Zhang and Y. Deng, *Biomacromolecules*, 2014, **15**, 2540-2547.
41. Y. Zhan, M. Lavorgna, G. Buonocore and H. Xia, *J. Mater. Chem*, 2012, **22**, 10464.
42. J. Melcher and G. Taylor, *Annu. Rev. Fluid. Mech*, 1969, **1**, 111-146.
43. J. F. Delamora and I. G. Loscertales, *J. Fluid Mech.*, 1994, **260**, 155-184.
44. M. Enayati, M.-W. Chang, F. Bragman, M. Edirisinghe and E. Stride, *Colloids. Surf. A*, 2011, **382**, 154-164.
45. C. J. Young, L. A. Poole-Warren and P. J. Martens, *Biotechnol. Bioeng.*, 2012, **109**, 1561-1570.
46. N. Chen and Q. Pan, *ACS nano*, 2013, **7**, 6875-6883.
47. C. H. Yang, C. Y. Wang, K. S. Huang, C. S. Yeh, A. H. Wang, W. T. Wang and M. Y. Lin, *PloS one*, 2012, **7**, e49329.
48. H. Zhang, I. Hussain, M. Brust, M. F. Butler, S. P. Rannard and A. I. Cooper, *Nat. Mater*, 2005, **4**, 787-793.
49. Y. Long, C. Zhang, X. Wang, J. Gao, W. Wang and Y. Liu, *J. Mater. Chem*, 2011, **21**, 13934.
50. Y. W. Zhu, S. Murali, M. D. Stoller, A. Velamakanni, R. D. Piner and R. S. Ruoff, *Carbon*, 2010, **48**, 2118-2122.
51. H. Hu, Z. Zhao, Q. Zhou, Y. Gogotsi and J. Qiu, *Carbon*, 2012, **50**, 3267-3273.
52. D. A. Dikin, S. Stankovich, E. J. Zimney, R. D. Piner, G. H. Dommett, G. Evmenenko, S. T. Nguyen and R. S. Ruoff, *Nature*, 2007, **448**, 457-460.
53. J. Du, X. Lai, N. Yang, J. Zhai, D. Kisailus, F. Su, D. Wang and L. Jiang, *ACS nano*, 2010, **5**, 590-596.
54. Y. Li, X. Lv, J. Lu and J. Li, *J. Phys. Chem. C*, 2010, **114**, 21770-21774.
55. A. C. Ferrari and D. M. Basko, *Nat. Nanotechnol*, 2013, **8**, 235-246.
56. Z. Xu, Y. Zhang, P. Li and C. Gao, *ACS Nano*, 2012, **6**, 7103-7113.
57. H. Sun, Z. Xu and C. Gao, *Adv. Mater.*, 2013, **25**, 2554-2560.
58. Z. Niu, J. Chen, H. H. Hng, J. Ma and X. Chen, *Adv. Mater.*, 2012, **24**, 4144-4150.
59. Y. He, Y. Liu, T. Wu, J. Ma, X. Wang, Q. Gong, W. Kong, F. Xing, Y. Liu and J. Gao, *J. Hazard .Mater*, 2013, **260**, 796-805.
60. X. Dong, J. Chen, Y. Ma, J. Wang, M. B. Chan-Park, X. Liu, L. Wang, W. Huang and P. Chen, *Chem. Commun*, 2012, **48**, 10660.
61. H. Hu, Z. Zhao, Y. Gogotsi and J. Qiu, *Environ. Sci & Technol,* 2014, **1**, 214-220.
62. H. Li, L. Liu and F. Yang, *J. Mater. Chem. A*, 2013, **1**, 3446.
63. R. Li, C. Chen, J. Li, L. Xu, G. Xiao and D. Yan, *J. Mater. Chem. A*, 2014, **2**, 3057.
64. J. Bernal and J. Mason, *Nature*, 1960, **188**, 910-911.
65. K. Gotoh, *Nature*, 1974, **252**, 202-205.

Novel graphene oxide aerogel microspheres(GOAMs) with well-defined "Center-diverging microchannels" structures are obtained by a novel approach, i.e. combination of electrospraying and freeze-casting. A formation mechanism, i.e. radial–directional freezing-thawing was proposed. The reduced GOAMs exhibit excellent adsorption ability for various organic liquids and oils due to its highly hierarchical hydrophobic structure and randomly packing effect.